Stress effect on segregation and ordering in Pt–Ag nanoalloys

Alexis Front, Christine Mottet

IOP Publishing Journal of Physics: Condensed Matter
J. Phys.: Condens. Matter **33** (2021) 154006 (7pp) https://doi.org/10.1088/1361-648X/abe07a

Stress effect on segregation and ordering in Pt–Ag nanoalloys

Alexis Front[1] **and Christine Mottet**

Aix-Marseille University, CNRS, CINaM UMR 7325, Campus de Luminy, Marseille 13288, France

E-mail: mottet@cinam.univ-mrs.fr

Received 14 December 2020, revised 19 January 2021
Accepted for publication 27 January 2021
Published 1 March 2021

Abstract

We performed a theoretical study of the chemical ordering and surface segregation of Pt–Ag nanoalloys in the range of size from 976 to 9879 atoms (3.12 to 6.76 nm). We used an original many-body potential able to stabilize the $L1_1$ ordered phase at equiconcentration leading to a strong silver surface segregation. Based on a recent experimental study where nanoparticles up to 2.5 nm have been characterized by high transmission electron microscopy with the $L1_1$ ordered phase in the core and a silver surface shell, we predict in our model via Monte Carlo simulations that the lower energy configuration is more complicated with a three-shell alternance of Ag/Pt/Ag from the surface surrounding the $L1_1$ ordered phase in the core. The stress analysis demonstrates that this structure softens the local stress distribution inside the nanoparticle which contributes to reduce the internal energy.

Keywords: nanoalloys, segregation, chemical ordering, stress

(Some figures may appear in colour only in the online journal)

1. Introduction

Nanoalloys are commonly nanoparticles of alloys where both size and composition influence their structures and properties. They represent a very attractive and intensive domain of research from the last ten years with very interesting properties and potential applications in catalysis, plasmonics, magnetic data storage, biomarkers, drug delivery, cancer detection and treatment... [1, 2]. The variety of morphologies and structures as a function of their size is significantly enhanced with the chemical organization of the different species inside the nanoparticles and especially between the surface and the core. Indeed, the surface is the place where segregation potentially occurs, whereas the core is the place where bulk alloy phases with finite size effects are found. The chemical arrangement at the surface plays a major role in catalysis whereas optical and magnetic effects are sensible to the overall chemical configuration. Whereas a large panel of systems have been studied these last twenty years, only very recently the Pt–Ag one has been the subject of both experimental and theoretical studies. As the Pt–Cu prototype, the Pt-Ag alloy orders at equiconcentration according to the original $L1_1$ phase characterized by an alternation of pure atomic layers in the (111) orientation. Whereas previous theoretical studies [3, 4] did not mention the specific $L1_1$ phase in the nanoparticles, experimental observations using high resolution transmission electron microscopy have shown for the first time the ordered $L1_1$ nanophase in small Pt–Ag nanoparticles [5]. In collaboration with theoretical analysis coupling *ab initio* calculations and Monte Carlo simulations, this study concludes that Pt–Ag nanoalloys are characteristic of a reversed size-dependent stabilization of ordered nanophases because the fully ordered $L1_1$ is better stabilized in small nanoparticles (up to 2.5 nm) than in larger ones, in which the ordered phase breaks in multiple domains or is interrupted by faults. The smaller Pt–Ag nanoalloys are composed of a silver shell and a $L1_1$-core but with increasing size, because of increasing stress coming from the misfit between the pure silver surface shell and the orthorhombic $L1_1$ ordered core, there are some defects that we would like to analyze here from a theoretical point of view. We have already showed that above one thousands

* Author to whom any correspondence should be addressed.

[1] Present address: Laboratoire d'Etude des Microstructures, ONERA-CNRS, UMR104, Université Paris-Saclay, BP 72, 92322 Châtillon cedex, France.

atoms, Monte Carlo simulations predict another structure with a Pt-subsurface shell between the silver shell and the $L1_1$-core which allows to release the stress [5]. In the present study we extend our simulations to other possible defects notably in the $L1_1$-core in order to compare and analyze, in term of stress release, different faulted structures as they were observed in the experiments.

In bulk alloy, the Pt–Ag system is a particular system which displays a phase separation at high temperature and an ordered compound at equiconcentration with the $L1_1$ phase [6, 7]. This phase is quite scarce in the fcc alloys because it displays an alternation of pure planes in the (111) direction instead of the more usual $L1_0$ phase that we find in most of the other fcc alloys with ordering tendency for which the alternation of pure atomic planes is in the (100) direction. The $L1_1$ phase has been established by *ab initio* calculations [8] and we built an original many-body potential for the Pt–Ag systems fitted on density functional theory (DFT) calculations. This article is composed of four sections including this introduction. In the next section we detail the energetic model, the Monte Carlo simulations and the stress analysis method. Then we give the results in section 3 before to conclude.

2. Energetic model and simulation methods

2.1. Many-body potential for Pt–Ag system

The Pt–Ag system has the particularity to form an ordered $L1_1$ phase at the equiconcentration which is an alternation of pure (111) atomic layers as in the better known Cu–Pt system [9] (see figure 1). These particular phase is stabilized by the second neighbors effective pair interactions in a tight binding Ising model [10, 11] where the Halmiltonian is written as follows in bulk alloys [12]:

$$H^{\mathrm{TBIM}} = \sum_{n,m} p_n p_m V_{nm}. \tag{1}$$

The effective pair interactions between sites n and m, $V_{nm} = \frac{1}{2}(V^{AA} + V^{BB} - 2V^{AB}) = V^{1,2,\cdots}$ characterize chemical ordering with n, m being 1st, 2nd, …neighbors. Hence $V^1 > 0$ means the system has the tendency to order whereas $V^1 < 0$ means the system makes phase separation. For the usual $L1_0$ phase which is an alternation of pure atomic layers in the (001) direction (see figure 1), $V^1 > 0$ is sufficient to stabilize the ordered phase. For the $L1_1$ phase, we have to satisfy the relation $V^2 > V^1/2$ if $V^1 > 0$ or $V^2 > -V^1$ if $V^1 < 0$ (see reference [12]). This Ising model has been a guide to build our energetic model based on a semi-empirical potential derived from the electronic structure in the tight binding approximation: the so-called second moment approximation [13] (TB–SMA) of the density of states. The TB–SMA interatomic potential has been modified to stabilize the specific $L1_1$ phase at the equiconcentration by adding an attractive contribution with a gaussian shape localised at the second neighbors distance only for the mixed interactions. This original potential is

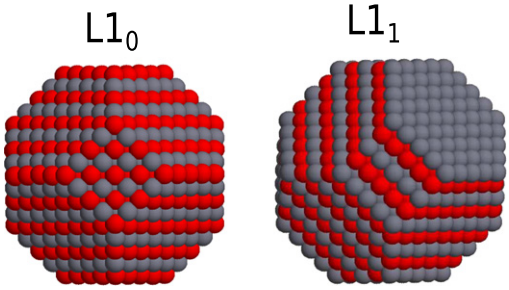

Figure 1. Illustration of the $L1_0$ and $L1_1$ phases.

written as follows [5]:

$$E_i^a = -\sqrt{\sum_{j,r_{ij}<r_{ab}^3} \xi_{ab}^2 e^{-2q_{ab}\left(\frac{r_{ij}}{r_{ab}^0}-1\right)}} - \sum_{j,r_{ij}<r_{ab}^3} G e^{-\frac{(r_{ij}-r_2)^2}{2\sigma^2}} + \sum_{j,r_{ij}<r_{ab}^3} A_{ab} e^{-p_{ab}\left(\frac{r_{ij}}{r_{ab}^0}-1\right)}, \tag{2}$$

where the first two terms represent the attractive part with the classical square root dependence with the neighboring atoms and a gaussian contribution centered at the second neighbors distance, then the last term, the repulsive part, with a pairwise Born Mayer form. In this expression, r_{ij} is the distance between the atom at site i and their neighbors at site j, r_{ab}^3 is a cutoff distance at the third neighbor and r_{ab}^0 is the first neighbor distance depending on the nature of the atoms. Then, p_{ab}, q_{ab}, A_{ab}, ξ_{ab}, G and σ are six parameters which are fitted to experimental and DFT data of lattice parameters, cohesive energies, surface energies, elastic constants for the pure metals and to the solution energies and formation energies of ordered phases for the mixed interactions.

DFT calculations have been performed using the VASP code developed on plane waves and using the generalized gradient approximation (GGA) with the Perdew-Wang 91 functional [14] and PAW pseudopotentials [15] implemented by Kresse and Joubert [16]. The calculations consider s and d electrons of each metal with a cutoff in energy equal to 600 eV in the plane waves basis. The Brillouin zone is integrated within the Monkhorst–Pack method. We calculated the lattice parameter, cohesive energies and surface energies of the pure metals and compared them to the experimental values (see table 1). The lattice parameters are overestimated whereas the cohesive energies are underestimated by the DFT calculation which is a usual result using GGA functional. As a consequence, the surface energies also are underestimated, keeping the same difference between the two metals which is an important driving force for surface segregation. The p_{aa}, q_{aa}, A_{aa}, ξ_{aa} parameters for the pure metals have been fitted to the DFT values of the lattice parameters and cohesive energies and to the experimental values of the elastic constants. Then

Table 1. Lattice parameter a, cohesive energy E_{coh}, surface energies γ and elastic constants B, c_{44} and c' for Pt and Ag in DFT–GGA and TB–SMA calculations, and from experiments: Kittel, *Introduction to solid state physics* (Wiley 1996) for lattice parameter and cohesive energy; De Boer *et al*, *Cohesion in metals*, North-Holland, Amsterdam (1988) for surface energies; Simmons and Wang, *Single crystal elastic constants and calculated aggregates properties* (MIT 1971) for elastic constants.

		a (Ang.)	E_{coh} (eV/at.)	$\gamma^{(111)}$ (J m^{-2})	$\gamma^{(100)}$ (J m^{-2})	B (GPa)	c_{44} (GPa)	c' (GPa)
Pt	DFT	3.98	−5.53	1.50	1.85	—	—	—
	Exp.	3.92	−5.86	—	2.48	288	77	52
	SMA	3.98	−5.53	1.20	1.36	203	105	37
Ag	DFT	4.16	−2.725	0.77	0.83	—	—	—
	Exp.	4.09	−2.95	—	1.25	108	56	20
	SMA	4.16	−2.725	0.63	0.73	95	52	18

Table 2. Formation enthalpies ΔH of the ordered $L1_1$ and $L1_0$ phases and their lattice mesh characteristics (c/a). For the $L1_1$ phase, c axis is perpendicular to (111) planes whereas in the $L1_0$ phase, c axis is perpendicular to the (100) planes. In each case we choose the c axis along the direction of the alternation of pure atomic planes. Dissolution energies of one impurity of Ag in Pt, Pt(Ag) and of Pt in Ag, Ag(Pt).

PtAg	Method	$L1_1$	$L1_0$	Pt(Ag)	Ag(Pt)
ΔH (eV/at.)	DFT–GGA [8]	−0.039	0.063	—	—
	DFT–GGA (present study)	−0.051	0.041	0.140	−0.040
	TB–SMA	−0.213	0.063	0.004	−0.560
c/a	DFT–GGA [8]	—	—	—	—
	DFT–GGA (present study)	1.03	1.06	—	—
	TB–SMA	1.05	1.08	—	—

Table 3. TB-SMA interatomic potential parameters. $r^3_{\alpha-\beta}$ represents a cutoff distance around the 3rd neighbors where the effective SMA potential is connected to a polynomial form of the potential between third and fourth neighbors distance and $r^4_{\alpha-\beta}$ represents the cutoff distance around the 4th neighbors where the potential is zero.

$\alpha-\beta$	$p_{\alpha-\beta}$	$q_{\alpha-\beta}$	$A_{\alpha-\beta}$	$\xi_{\alpha-\beta}$	$G_{\alpha-\beta}$	$\sigma_{\alpha-\beta}$	$r^3_{\alpha-\beta}$	$r^4_{\alpha-\beta}$
Pt–Pt	10.7960	3.1976	0.1993	2.2318	—	—	4.8745	5.6286
Ag–Ag	11.7240	2.8040	0.0748	1.0064	—	—	5.0949	5.8831
Pt–Ag	11.2600	3.0008	0.1456	1.5920	0.0440	0.0350	5.0949	5.6286

we calculated the surface energy to check the TB-SMA potential as reported in table 1. Finally we calculated the formation enthalpy of the ordered $L1_1$ and $L1_0$ phases, for fitting the mixed interactions. The results are reported in table 2 together with the results obtained by Sluiter *et al* [8]. In our calculations we optimized the lattice mesh which changes from fcc to rhombohedral in the $L1_1$ phase and tetragonal in the $L1_0$ phase. As this optimization is not mentioned in the study by Sluiter *et al* [8], this could justify the slight difference in energy between our results and theirs.

The parameters p_{ab} and q_{ab} for the mixed interactions are the average of the ones for the pure metals. The other four parameters A_{ab}, ξ_{ab}, G and σ are fitted to the formation enthalpies of the ordered $L1_1$ and $L1_0$ phases and to the solution energies of one impurity in the matrix of the other metal. We can see on table 2 that the best values obtained with the TB-SMA for the formation enthalpies and the dissolution energies are sometimes far from the reference we want to fit. This is a difficulty of the model which is quite simple to reproduce all the physical quantities. What we notice is that the formation enthalpy of the $L1_1$ phase is multiplied by a factor 4 as compared to the DFT value, which was necessary to effectively stabilize it in Monte Carlo simulations. Then the dissolution energies respect at least the sign, which means it is favorable to dissolve Pt in Ag but not Ag in Pt, which is indeed in agreement with the bulk alloy phase diagram [7, 8]. The TB-SMA parameters obtained after the fit are reported in the table 3.

2.2. Monte Carlo simulations

Then we use Monte Carlo simulations in the canonical or semi-grand canonical ensemble to optimize the chemical configuration of the clusters. In canonical, keeping the same concentration, we propose random atomic exchange of atoms of different species, and small random atomic displacements around each atom position. The chemical composition, the pressure, the temperature and the total number of atoms remain

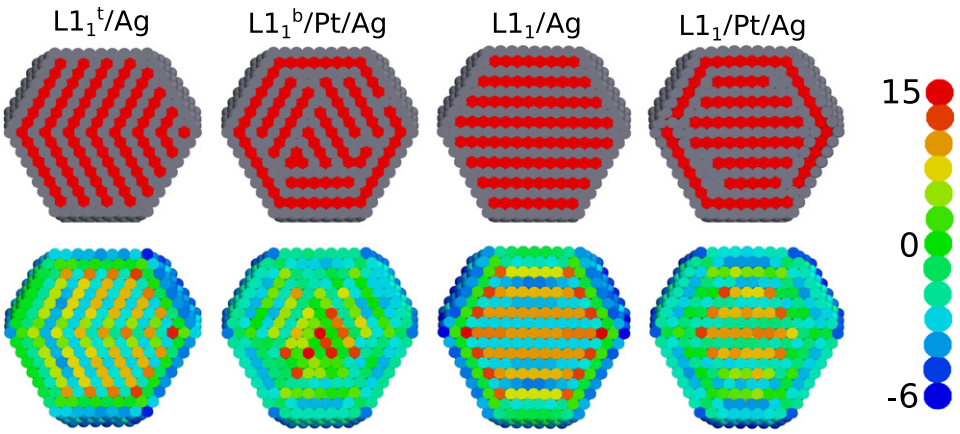

Figure 2. TOh_{2951}: snapshot of different configurations (Pt atoms in red and Ag atoms in gray, on the first line) at 0 K at $c_{Ag} = 0.633$ and their associated stress map (on the second line) in color code from -6 GPa for tensile stress to 15 GPa for compressive stress. $L1_1^t/Ag$ corresponds to a twining of the $L1_1$ phase in the core, $L1_1^b/Pt/Ag$ to multiple phase boundaries containing a Pt-subshell, $L1_1/Ag$ to the perfect $L1_1$-core and $L1_1/Pt/Ag$ to a $L1_1$-core surrounded by a Pt-subshell.

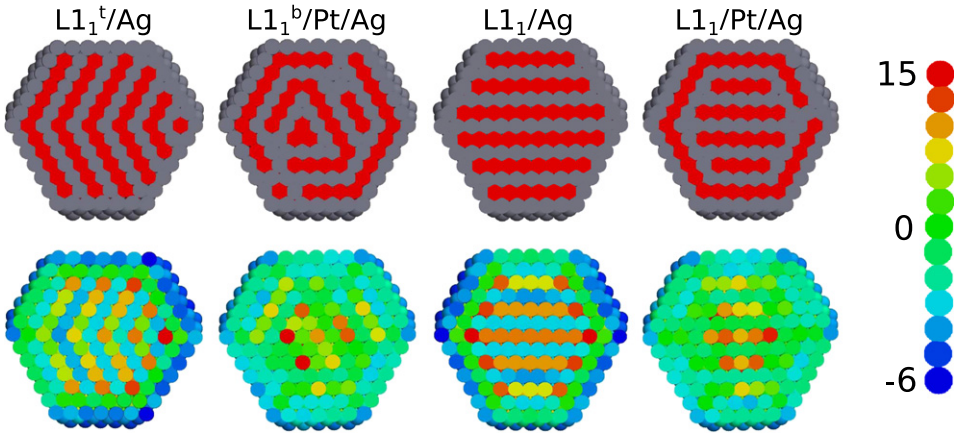

Figure 3. Same as figure 2 for TOh_{1289} and $c_{Ag} = 0.673$.

constant, and the atomic and chemical configuration evolves toward the equilibrium configuration. In semi-grand canonical ensemble, we keep the chemical potential difference between the two species as a reservoir of matter and we propose random permutation of species (one atom of type A is permuted in type B at the same site), then we propose small random atomic displacements around each atom position as in canonical ensemble. The chemical potential difference, the pressure, the temperature and the total number of atoms remain constant, but the chemical configuration and concentration evolve toward the equilibrium chemical configuration.

The Metropolis [17] sampling ensures attainment of a Boltzmann distribution of the chemical configurations at equilibrium, this means when the number of Monte Carlo trials is sufficient to get reliable averages of physical quantities. In the Metropolis Monte Carlo, a trial is accepted if it lowers the total energy of the system. If not, it can still be accepted with the probability equal to $e^{(-\frac{\Delta E}{kT})}$ where ΔE is the energy difference between the configurations before and after the trial, k being the Boltzmann constant and T the temperature.

2.3. Local stress analysis

Stress map inside the nanoparticles are determined on the atomic structures which have been relaxed in their minimum of energy at 0 K by quenched molecular dynamics. The quenched molecular dynamics consists in a classical molecular dynamics in microcanonic ensemble which means keeping number af atoms, the global pressure, and the total energy (potential + kinetic) constant. But instead of letting the system evolves freely, we cancel the velocity of one atom when its velocity is opposite to the atomic force (which brings it back to the local potential energy minimum). This procedure tends to quench the system toward the nearest local energy minimum of a given structure. The atomic stress is characterized by the following expression giving the variation of the energy as a function of the local deformations of the interatomic distances r_{ij} (expressed in eV) according to the expression of an hydrostatic pressure [18]:

$$p_i = -\frac{1}{3}\sum_j \frac{dE_{ij}}{dr_{ij}} r_{ij}. \quad (3)$$

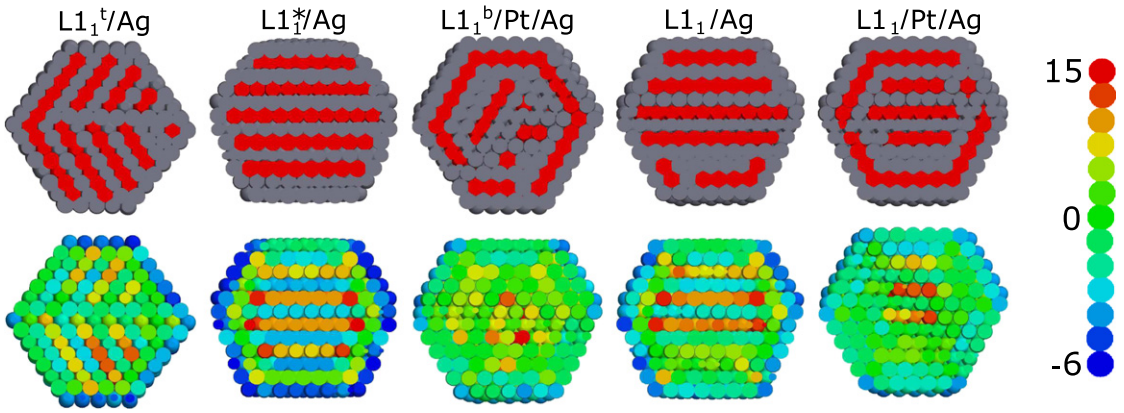

Figure 4. Same as figure 2 for TOh_{976} with even number of atomic layers and $c_{Ag} = 0.700$. Because of the even number of atomic layers, the perfect $L1_1$-core, noted $L1_1/Ag^*$ here, is no more the reference structure because the introduction of one stacking fault stabilizes the structure to be compared to the equivalent structures in figures 2 and 3.

3. Results and discussion

We studied nanoparticles in the shape of Truncated Octahedron (TOh), which corresponds to the equilibrium morphology on an fcc lattice on a large range of size [19, 20]. The composition of the nanoalloys is the one which satisfies the chemical configuration corresponding to a perfect $L1_1$ ordered phase in the core and a pure silver surface shell (called '$L1_1$/Ag'). This composition is not far from the equiconcentration but rather enriched in silver because the surface shell is Ag pure. Moreover this concentration depends on the cluster size. We consider possible chemical faulted structures that appear by canonical Monte Carlo simulations. To point out these different configurations, we choose three sizes. Firstly two clusters of 2951 and 1289 atoms, containing an odd number of layers, are compared to enlighten a possible size effect. Secondly, we consider a cluster of 976 atoms characterized by an even number of layers which leads to possible chemical stacking faults. As illustrated on the figure 2 ($N = 2951$) and figure 3 ($N = 1289$), four configurations keeping an Ag-shell with a different core are characterized: a single phase boundary structure corresponding to a twining of the $L1_1$ to accommodate it along two adjacent (111) facets ($L1_1^t$/Ag), a $L1_1$-core with multiple phase boundaries containing a Pt-subshell ($L1_1^b$/Pt/Ag), a perfect $L1_1$-core ($L1_1$/Ag) and a $L1_1$-core surrounded by a Pt-subshell ($L1_1$/Pt/Ag). In the case of an even number of layers (see figure 4, $N = 976$), as we will explicit later, the perfect $L1_1$-core is no more the best structure to take as reference because the even number of layer induces the introduction of a stacking fault in the $L1_1$-core. So for the cluster of 976 atoms (figure 4) with an even number of atomic layers, the $L1_1$ phase in the core may display some stacking faults, but we will consider these faulted core in the same way as the other unfaulted structures with odd number of layers (figures 2 and 3).

Starting from $L1_1$/Ag and $L1_1^t$/Ag structures using Monte Carlo simulations in canonical ensemble, we heat to check the stability of these phases. Then starting from Pt pure or Ag pure cluster, using semi-grand canonical ensemble, we seek for similar configurations at the same concentration. To determine the local minima at 0 K for each given chemical configuration, we quench the system by quenched molecular dynamics. Then we compared the energy of the different structures described above to the $L1_1$/Ag one used as a reference. As illustrated by ΔE(i) in table 4, a minus sign means that the structure *i* is more stable than the structure $L1_1$/Ag. Finally, we do a stress analysis to investigate the difference of stability between structures. We plotted the local stress map corresponding to each structures.

Compared to the energy of the $L1_1$/Ag structure, we can see on table 4, that a twining phase boundary ($\Delta E(L1_1^t/Ag)$) costs more than multiple phase boundaries ($\Delta E(L1_1^b/Pt/Ag)$). By decreasing cluster size the twining structure is less and less stable whereas the multiple boundaries structure is more and more stable up to become more stable than the $L1_1$/Ag structure at size equal to 976. However, in this range of size, the $L1_1$/Ag structure is not the most stable one. The Pt-subsurface segregation allows a significant energy gain which increases with decreasing size. At this point we can notice that, as our model overestimates the stability of the $L1_1$ phase (its formation enthalpy is four times the DFT value, see table 2), the fact that this phase is not perfectly stabilized in clusters makes even more robust our results. To understand why such phase is not easily stable in clusters, we have investigated the local pressure in the nanoparticles.

We observe in figures 2 and 3 that the structure $L1_1$/Ag presents an alternation of compressed and tensile layers in the $L1_1$-core along a (111) direction. A Pt-subsurface segregation as well as Ag enrichment in the third shell allow to release the inhomogeneous stress, which explains the energy gain. The subsurface segregation of the smallest element has already been observed in many systems starting from the theoretical study by Bochicchio *et al* [21] on systems with phase separation tendency. But it also appeared in nanoalloys with the ordering tendency as in Pt–Pd nanoalloys [22]. With the Pt–Ag system, we are just between the two tendencies since it presents both large phase separation areas between solid solutions of Pt-rich and Ag-rich domains but it also forms a chemical ordered phase at equiconcentration. This leads both to a strong silver surface segregation in coexistence with the ordered $L1_1$ phase in the core. Both the misfit between the

Table 4. Difference ΔE(i), in meV/at., between the energy of a considered structure *i* and the $L1_1$/Ag one (as illustrated on the figures 2–4) quenched at 0 K. A minus sign means that the structure *i* is more stable than the structure $L1_1$/Ag; in bold, the most stable configuration.

N	N_{Ag}	$\Delta E(L1_1^t/Ag)$	$\Delta E(L1_1^b/Pt/Ag)$	$\Delta E(L1_1/Ag)$	$\Delta E(L1_1/Pt/Ag)$
2951	1869	4.87	1.65	0	**−0.93**
1289	867	5.77	0.51	0	**−1.38**
976	685	8.41	−0.99	0	**−2.15**

Table 5. Difference ΔE between the energy of the $L1_1$/Pt/Ag structure and a multiple phase boundaries $L1_1^b$/Pt/Ag in meV/at. A minus sign means that the structure $L1_1$/Pt/Ag is the most stable.

	976	1289	2951	4249	7573	9879
ΔE (meV/at.)	−1.16	−1.89	−2.59	−3.35	−5.02	−9.03

core and the surface shell, and the rhombohedral deformation associated with the $L1_1$ phase makes the structure stressed.

Looking at the stress map on figure 4, Pt segregation on subsurface allows to release stress in the core, giving a homogeneous distribution of the internal stress for $L1_1^b$/Pt/Ag and $L1_1$/Pt/Ag. In the special case of an even number of atomic layers, the perfect $L1_1$-core noted $L1_1/Ag^*$ implies that the $L1_1$ phase ends by a silver plane which makes a kind of stacking fault with the silver surface shell. We found that this stacking fault costs less energy inside the core than between the core and the shell. This is why we introduce the stacking fault in the core of the reference structure $L1_1$/Ag. On the stress map we observe that the stacking fault in the core is more efficient to release the stress than the stacking fault located near the surface. It is finally surprising on the stress map to see that this is not precisely the silver plan in contact with the silver shell which is compressed in the $L1_1/Ag^*$ structure but it is rather the release of the compression on the stacking fault in the core in the $L1_1$/Ag structure where one Ag plane is almost fully relaxed (green in the stress map).

More generally, Pt-subsurface associated to Ag-subsubsurface allow to release the internal stress in the core which implies an energy gain. That is why the $L1_1$/Pt/Ag structure is stabilized. However, when size increases there is still an accumulation of stress in the core. A possible competition between this structure and multiple phase boundaries in the core may occur. To answer this question we have tested larger sizes up to 9879 atoms (around 7 nm) and compared the energies of the two structures. The results are reported on table 5 where we see rather an augmentation of the stability of the $L1_1$/Pt/Ag structure as compared to the other ones, with increasing size. We have to keep in mind that in the present study we fixed the composition to fit perfectly the $L1_1$/Ag structure which is certainly not the best one for such sizes. In perpective it could be interesting to explore other concentrations in order to optimize new possible chemical configurations. But what arises from this study is that the large $L1_1$ phase in the core coupled to a silver surface shell is not stable at large size and we have to investigate how to conciliate Ag surface segregation and core ordering in finite nanoparticles where stress plays a major role, and more and more with increasing the size.

4. Conclusions

To conclude, we have used a realistic many-body potential for the original Pt–Ag system to study the chemical ordering in truncated octahedron nanoalloys with a specific composition corresponding to the configuration observed by the experiments [5]. This configuration corresponds to an ordered $L1_1$-core with a pure silver surface shell. However among the experimental results some of them have reported some stacking faults that we have intentionally studied with our model. We found that neither the perfect $L1_1$/Ag structure, neither the twining or multiphase boundaries in the core are the best ones. In the whole range of size from 976 to 9879, including odd/even number of atomic layers in the core, the best configuration is the one made by a reduced $L1_1$ ordered phase in the core, surrounded by an alternance of Ag/Pt/Ag concentric shells from the surface, so-called $L1_1$/Pt/Ag structure. The local stress analysis revealed that this is the structure which allows to release sensibly the stress at the vicinity of the surface shell. This is a nice exemple of stress effect on ordering and surface segregation in nanoalloys. The comparison with experiments coming from high resolution transmission electron microscopy is still open since the precise zone in between the surface shell and the core is not completely resolved up today.

Acknowledgments

The authors warmly thank Bernard Legrand, Guy Tréglia and Riccardo Ferrando for fruitful discussions and acknowledge support from the International Research Network-IRN ‘Nanoalloys’ of CNRS. This work was granted access to the HPC resources of IDRIS under the allocation 2017-096829 mage by GENCI.

Data availability statement

All data that support the findings of this study are included within the article (and any supplementary files).

ORCID iDs

Christine Mottet https://orcid.org/0000-0002-7084-911X

References

[1] Ferrando R, Jellinek J and Johnston R L 2008 *Chem. Rev.* **108** 845
[2] Ferrando R, Johnston R L and Louis C 2015 *Phys. Chem. Chem. Phys.* 1727903
[3] Deng L, Deng H, Xiao S, Tang J and Hu W 2013 *Faraday Discuss.* **162** 293
[4] Che C, Xu H, Wen H, Gou G and Cheng D 2019 *J. Cluster Sci.* **31** 615
[5] Pirart J, Front A, Rapetti D, Andreazza-Vignolle C, Andreazza P, Mottet C and Ferrando R 2019 *Nat. Commun.* **10** 1982
[6] Hart G L W *et al* 2017 *Acta Mater.* **124** 325
[7] Durussel P and Feschotte P 1996 *J. Alloys Compd.* **239** 226
[8] Sluiter M H F, Colinet C and Pasturel A 2006 *Phys. Rev.* B **73** 174204
[9] Hultgren R, Desai P D, Hawkins D T, Gleiser M and Kelley K K 1073 *Selected Values of the Thermodynamic Properties of Binary Alloys* (Cleveland, OH: American Society of Metals)
[10] Tréglia G, Legrand B and Ducastelle F 1988 *Europhys. Lett.* **7** 575
[11] Khoutami A, Legrand B and Treglia G 1993 *Surf. Sci.* **287/288** 851
[12] Ducastelle F 1991 *Order and Phase Stability in Alloys Cohesion and Structure* de Boer F R and Pettifor D G (North-Holland: Elsevier)
[13] Rosato V, Guillopé M and Legrand B 1989 *Phil. Mag.* A **59** 321
[14] Perdew J P and Wang Y 1992 *Phys. Rev.* B **45** 13244
[15] Blöchl P E 1994 *Phys. Rev.* B **50** 17953
[16] Kresse G and Joubert D 1999 *Phys. Rev.* B **59** 1758
[17] Metropolis N, Rosenbluth A W, Rosenbluth M N, Teller A H and Teller E 1953 *J. Chem. Phys.* **21** 1087
[18] Kelires P C and Tersoff J 1989 *Phys. Rev. Lett.* **63** 1164
[19] Baletto F, Ferrando R, Fortunelli A, Montalenti F and Mottet C 2002 *J. Chem. Phys.* **116** 3856
[20] Zhu B, Guesmi H, Creuze J, Legrand B and Mottet C 2015 *Phys. Chem. Chem. Phys.* **17** 28129
[21] Bochicchio D and Ferrando R 2013 *Phys. Rev.* B **87** 165435
[22] De Clercq A, Giorgio S and Mottet C 2016 *J. Phys.: Condens. Matter.* **28** 064006